Prasanna K. Thwar[1]
Jennifer J. Linderman[1, 2]
Mark A. Burns[1, 2]

[1]Department of Chemical Engineering, University of Michigan, Ann Arbor, MI, USA
[2]Department of Biomedical Engineering, University of Michigan, Ann Arbor, MI, USA

Received May 22, 2007
Revised August 19, 2007
Accepted August 22, 2007

Research Article

Electrodeless direct current dielectrophoresis using reconfigurable field-shaping oil barriers

We demonstrate dielectrophoretic (DEP) potential wells using pairs of insulating oil menisci to shape the DC electric field. These oil menisci are arranged in a configuration similar to the quadrupolar electrodes, typically used in DEP, and are shown to produce similar field gradients. While the one-pair well produces a focusing effect on particles in flow, the two-pair well results in creating spatial traps against crossflows. Uncharged polystyrene particles were used to map the DEP force fields and the experimental observations were compared against the field profiles obtained by numerically solving Maxwell's equations. We demonstrate trapping of a single particle due to negative DEP against a pressure-driven crossflow. This can be easily extended to trap and hold cells and other objects against flow for a longer time. We also show the results of particle trapping experiments performed to observe the effect of adjusting the oil menisci and the gap between two pairs of menisci in a four-menisci configuration on the nature of the DEP well formed at the center. A design parameter, Θ, capturing the dimensions of the DEP energy well, is defined and simulations exploring the effects of different geometric features on Θ are presented.

Keywords:
Barriers / Direct current dielectrophoresis / Electrodeless dielectrophoresis / Field shaping / Trapping
DOI 10.1002/elps.200700373

1 Introduction

Dielectrophoresis (DEP) is a common method of manipulation of particles in flow in microfluidic devices [1–10]. Among all methods used for particle handling in continuous flow microfluidic systems, DEP offers a stable, electronically controllable, microfluidically self-contained, and scalable method to handle particles of widely varying electrical properties (charged or uncharged) along with the other advantages that typical electrophoresis offers [3, 11]. Since DEP does not require the sample to have specific properties (electrically conductive, magnetic, charged, dense, optically transparent, *etc.*), it is also useful for handling a wide range of particulate matter. Following the seminal work of Pohl and Crane [12], extensive theoretical and experimental efforts have brought a better understanding of using DEP in different forms and for different applications ranging from trapping and separating objects (particles, cells, and deoxyribonucleic acid (DNA)), manipulating fluids and suspended objects to patterning cell and particle assemblies for tissue engineering and sensing applications [1–4, 8–11, 13–31].

In DEP, a dielectric particle is differently polarized in a spatially nonuniform electric field resulting in positive dielectrophoresis (p-DEP), in which the particle is directed to locations of maximum field gradients or negative dielectrophoresis (n-DEP), in which the particle is directed to locations of minimum field gradients [32]. The Clausius–Mossotti factor (CM), a measure of the relative polarizability of the particle with respect to the medium, given by $CM = \varepsilon_p - \varepsilon_m/\varepsilon_p + 2\varepsilon_m$, determines whether a particle will experience p-DEP or n-DEP. Since the dielectric permittivity (ε) is a complex number, CM is highly dependent on the frequency of the DEP field applied. At high frequencies $\lim_{\omega\to\infty}|CM| = \varepsilon_p - \varepsilon_m/\varepsilon_p + 2\varepsilon_m$ and at very low frequencies, $\lim_{\omega\to 0}|CM| = \sigma_p - \sigma_m/\sigma_p + 2\sigma_m$ [32], where ε_p and ε_m are the dielectric constants of the particle and medium, respectively, and σ_p and σ_m are their conductivities.

The frequency dependence of CM is useful for controlling the movement of the particles towards and away from the electrodes. If CM >0 (*i.e.* $\varepsilon_p > \varepsilon_m$), the particles experience p-DEP forces and accumulate at electrode edges or electrode–liquid interfaces (highest field gradients) and if CM <0

Correspondence: Prasanna K. Thwar, 615 Davis Drive, Suite 800, Morrisville, NC 27560, USA
E-mail: prasanna.thwar@gmail.com
Fax: +1-919-287-9011

Abbreviations: CM, Clausius–Mossotti factor; **DEP,** dielectrophoresis/dielectrophoretic; **DNA,** deoxyribonucleic acid; **EDEP,** electrodeless dielectrophoresis; **n-DEP,** negative dielectrophoresis; **p-DEP,** positive dielectrophoresis; **PDMS,** polydimethyl siloxane

(*i.e.* $\varepsilon_p<\varepsilon_m$), the particles get repelled away from the highest field gradients due to n-DEP forces. Often the electrodes are designed such that the particles repelled from the electrode edges accumulate at the interelectrode gap [33, 34]. Charged particulate matter like DNA, proteins, and some types of cells exhibit p-DEP when they are suspended in solutions of low conductivity [2, 12, 19, 35]. Uncharged dielectric particles or cells with high membrane resistance suspended in aqueous solutions often exhibit n-DEP due to the high permittivity of water ($\varepsilon_m = 80$) [36]. Both p-DEP and n-DEP can be used depending upon the type of application and the nature of the particles and the suspending medium.

Traditionally, DEP is created by applying high-frequency alternating current (AC) voltage on planar microelectrodes or 3-D metallic structures patterned inside the microfluidic channel. While high field gradients can be obtained in such microelectrode geometries at relatively modest applied voltages, electrolysis at the electrode surfaces severely limits the maximum voltages that can be applied [37, 38]. In applications involving massive integration of particle manipulations, this also becomes complicated because of the need for complex electrode patterns, activation circuitry, and high-frequency AC sources and due to fringe fields created by interconnecting electrical lines. Fouling of electrode surfaces due to permanent particle deposition may also reduce the performance of these devices with time [39].

Recently, electrodeless dielectrophoresis (EDEP) has been developed as a viable alternative for regular DEP. In this method, voltage is applied using two end electrodes and the spatial variation in electric fields is created using insulating objects in the path of the electric field lines that render the straight field lines curved. Masuda *et al.* [40] demonstrated DEP fusion of two cells due to nonuniform fields created at the narrow restriction between two insulating surfaces. Chou *et al.* [19] demonstrated trapping of ssDNA and dsDNA using "EDEP" wherein local field maxima are created by squeezing the electric field through constrictions in an insulating channel. Cummings and Singh [41] used insulating posts in the flow path to generate "streaming DEP" and "trapping DEP" for different voltages applied. Since then, EDEP has been used for separating particles [30], DNA [42], proteins [43], bacterial, and viral cells [44–47]. Zhang *et al.* [48] presented the design of a circular EDEP microdevice based on a circular channel. Recently, Barbulovic-Nad *et al.* [49] used oil as an insulating post for creating DEP forces that caused continuous separation of particles based on size in a flowing stream. Applying similar concepts of shaping electric fields, Demierre *et al.* [50] demonstrated EDEP by creating equipotential surfaces that act as "liquid electrodes".

We present an EDEP method where local spatial nonuniformity in electric field is created using oil menisci as field-shaping insulating barriers. By positioning the oil menisci appropriately, we demonstrate DEP potential wells that can be used to focus the particle flow or trap single/multiple particles, respectively. While our method possesses the advantages of other EDEP methods like the elimination of electrolysis in the microchannel, electrode fabrication, and complex circuitry, it also provides an adjustable and reconfigurable method of controlling the location and extent of trapping locations as the oil menisci can be precisely regulated to produce appropriate field patterns. This method can be useful for applications like flow focusing, particle sorting, particle/cell assembly, DNA or protein concentration, sample preparation for further analysis in integrated devices.

2 Theory

The DEP force is the force exerted on a dielectric particle due to the induction of dipole moments by a nonuniform electric field. The net electric force on a spherical dielectric particle within a static electric field **E** is given [34] by

$$\mathbf{F}_{\mathrm{DEP}} = \frac{1}{4}\pi\varepsilon_m d^3 Re\left(\mathrm{CM}(\omega) \times \nabla\mathbf{E}^2\right) \tag{1}$$

where ε_m refers to the dielectric constant of the medium and CM (ω) refers to the frequency-dependent CM. If the particle is nonconductive and the medium is conductive, then Eq. (1) can be rewritten for a spherical particle in a direct current (DC) field as

$$\mathbf{F}_{\mathrm{DEP}} = -\frac{\pi}{8}\varepsilon_m d^3\left(\nabla\mathbf{E}^2\right) \tag{2}$$

Thus, nonconductive particles are directed away from locations of maximum field gradient (n-DEP). In a conservative force field where the potential energy is merely the spatial integral of the force field (*i.e.* $U = -\int_V FdV$), the potential energy seen by a particle in an n-DEP field can be simply given as

$$U_{\mathrm{DEP}} = \frac{\pi}{8}\varepsilon_m d^3\mathbf{E}^2 \tag{3}$$

While the DEP energy profile due to a field **E** (Eq. 3) is useful in determining the potential wells and the final locations of the particles, the magnitude and direction of DEP forces can be estimated using Eq. (2).

A particle under flow experiencing DEP may also experience other forces: drag, buoyancy, and Brownian forces. The net force acting on a particle is given by

$$\mathbf{F}_{\mathrm{net}} = \mathbf{F}_{\mathrm{DEP}} + \mathbf{F}_{\mathrm{Drag}} + \mathbf{F}_{\mathrm{Buoyancy}} \tag{4}$$

where, for a sphere,

$$\mathbf{F}_{\mathrm{Drag}} = 3\pi d\mu\left(\frac{4v_{\max}}{h}\right)F^* z \tag{5}$$

where "d" is the diameter of the particle, μ is the viscosity of the fluid medium, z is the distance of the particle from the wall, $v_{\max}$ is the velocity of the fluid at the middle of the channel, h is the height of the microfluidic channel, and F^* is a dimensionless factor accounting for the wall effects.

$\mathbf{F}_{\text{Buoyancy}}$ is given by

$$\mathbf{F}_{\text{Buoyancy}} = \frac{2}{3}\pi d^3 g\left(\rho_p - \rho_m\right) \tag{6}$$

where ρ_p is the density of the particle and ρ_m is the density of the fluid medium. Submicrometer particles may also experience random Brownian motion due to thermal forces characterized by a diffusion constant D, given by

$$D = \frac{kT}{3\pi\mu d} \tag{7}$$

While this may limit deterministic motion due to DEP for submicrometer particles, larger particles will not be affected significantly.

For trapping a particle at a specific location, the net force acting on the particle should be zero (*i.e.* $\mathbf{F}_{\text{net}} = \mathbf{0}$). Under laminar flows in microfluidic geometries, the drag forces are small (for $v_{\max} = 100$ μm/s, $d = 10$ μm, and $\mu = 1$ cP, $\mathbf{F}_{\text{drag}} \sim 10$ pN) and are usually present only in the direction of flow. The buoyancy forces can be minimized by density matching the fluid medium with additives. The DEP force fields are designed in such a way that the resultant $\mathbf{F}_{\text{DEP}}$ balances these disruptive forces.

3 Materials and methods

3.1 Polydimethylsiloxane device fabrication and assembly

Different channel designs were made using L-Edit program and the electronic designs were later translated into positive photomasks, made of either transparencies or glass coated with Cr and photoresist, with sharp contrast between the transparent and opaque regions. Negative photoresist SU8 2050 was spun on 4-inch 500 μm thick borofloat glass wafers and exposed to 365 nm UV for 120 s. The developed wafer with SU8 features were measured to be of 60–70 μm thickness. Glass posts of 1.5 mm diameter and 1 cm height were glued using 5 min epoxy onto the reservoir regions on SU8 where holes were needed. The wafer with SU8 features and the glass posts was then glued to a base plate made of glass along with a 1 cm-thick spacer to form a mold for polydimethyl siloxane (PDMS). Well-mixed Sylgard 184 PDMS mix with a precursor/initiator ratio of 10:1 was poured on to the mold, degassed, and cured for 2 h at 65°C. After curing, the PDMS cast was detached from the mold and the glass posts were carefully removed from the PDMS cast to leave behind perfect loading holes. The diced PDMS sides were then cleaned with ethanol, air-dried, and surface-activated by exposure to UV ozone for 20 min. Fully sealed microfluidic devices were then assembled by attaching this surface-activated PDMS sides to microscopic glass slides, also surface-activated by UV ozone, and kept under mild mechanical pressure for 2 h in 60°C. The devices were rinsed with ethanol before filling it with the experimental solutions to ensure proper wetting of the channel surfaces.

3.2 Experimental liquids

Ten micrometers of green fluorescent polystyrene particles (excitation λ: 469 nm and emission λ: 509 nm) with a specific gravity of 1.05 and suspended as 1% solids suspension were purchased from Duke Scientific (Fremont, CA). YG carboxylate-modified fluoresbrite particles (1.5 and 1.0 μm; excitation λ: 441 nm and emission λ: 486 nm) were purchased as 2.5% solids suspension from PolySciences (Warrington, PA). The suspending medium for the experiments was prepared with 20% glycerol solution for density-matching the polystyrene particles to prevent the particles from settling during the course of experiments and Tris HCl was added to make a final concentration of 0.001 M that is fairly conductive (0.05 S/m). The experimental suspensions were prepared by adding 100 μL of particle suspension obtained from the manufacturer to 1 mL of the suspending medium. Mineral oil (for molecular biology from Sigma–Aldrich; Sp. Gravity: 0.84 and viscosity ~25 cSt) was the oil used in all the experiments.

3.3 Image capture and processing

The DEP behavior of the particles under different electric field conditions was captured under a stereoscope both under bright field illumination and fluorescent conditions using a color digital camera and recorded as movies either on a hard drive or a VCR tape. For fluorescent microscopy, a UV light source (emission λ = 365 nm) was used to illuminate the fluorescent particles. The recorded movies were then converted to individual images and processed using Image J. Typically, the color fluorescent images were converted to 8-bit RGB images and then a particular threshold intensity was chosen as cutoff to convert the gray pixels to black or white values based on their intensities. Specific plugins were downloaded from Image J documentation webpage (http://rsb.info.nih.gov/ij/plugins/index.html) for calculating the area covered by pixels with intensities beyond a particular value at a specific region of interest in an image stack and the XY coordinates of the centroids of those areas.

3.4 Simulation of DEP force profiles

We performed numerical simulations to understand our experimental data of the DEP behavior of particles and also to predict the effect of different geometrical parameters on the dimensions of the DEP well.

From Maxwell equations, the electric field $\mathbf{E}$ follows

$$\nabla\mathbf{E} = \frac{\rho_e}{\varepsilon_m} \tag{8}$$

where ρ_e is the free charge density of the medium and ε_m its permittivity. For a homogeneous dielectric, this can be converted into Laplace form for the electric potential Φ as

$$\nabla^2\Phi = 0 \tag{9}$$

In our simulations, Eq. (9) was solved for the specific geometry of the electrodes and voltages applied (Neumann boundary conditions) using the commercial electromagnetic simulation program Maxwell 2D (Ansoft Corporation, Pittsburgh, PA). For EDEP, the same procedure was followed, except that the electrodes were replaced by insulating oil menisci. At the menisci, $\mathbf{E} = 0$ and the initial field across the main channel was specified using the values of voltages applied at both the ends. The spatially nonuniform field strength data matrix $\mathbf{E}$ was then calculated as the spatial derivative of the electric potential Φ. We then used Eq. (3) to determine the DEP energy field and compare different conditions of regular DEP and EDEP in this paper. For estimating the magnitude of particle holding forces due to DEP, we used the scalar form of Eq. (2).

3.5 Design and basic operation

In our device, the spatial nonuniformity of the DC electric field is rendered by one or two pairs of insulating oil menisci that protrude into a main channel along the length of which the DC field is applied. A schematic of the device is shown in Fig. 1. The main channel is 5 cm long and 300 μm wide and has two reservoirs at the end, each of volume ~375 nL. Four side channels situated as four corners of a rectangle, which deliver the insulating oil, open into the main channel that contains the particle suspension. The width of the channels (150–300 μm) and the gap between them (300–450 μm) is varied across the different designs. The design also features two side channels (75 μm wide) that would provide the fluidic vent for the particles under electrophoresis in the main channel. However, these channels were not used in the actual experiments and were sealed to prevent liquid entry.

In a typical experiment, the fully sealed PDMS-glass device is mounted on a stereoscope platform. The channel network is rinsed with ethanol and then filled with a homogenous particle suspension. The suspension is usually sonicated before use to resuspend the particles aggregated or settled due to gravity. Four syringes filled with oil are connected through polyethylene tubing and fluidic interconnects to the four side channels. The plungers of the syringe pumps are pushed in slowly to fill the oil and form menisci at the opening where the side channels join the main channel. The protrusion of the oil menisci in the main channel can thus be individually adjusted. The hydrophobic PDMS surfaces on three sides of the channels are easily wetted by the oil and hence the challenge frequently encountered was to maintain the menisci at the same level throughout the device operation. Care was taken to prime the oil tubing such that there was no backpressure or air traps that could potentially affect the menisci. We used the same devices for both 1-D and 2-D DEP experiments. For experiments with only one pair of opposing oil menisci (1-D DEP), the protrusion of the other pair of menisci was restricted.

4 Results and discussion

4.1 Design and construction of DEP fields

Two insulating oil menisci, facing each other and protruding into a channel, constrict the otherwise straight field lines due

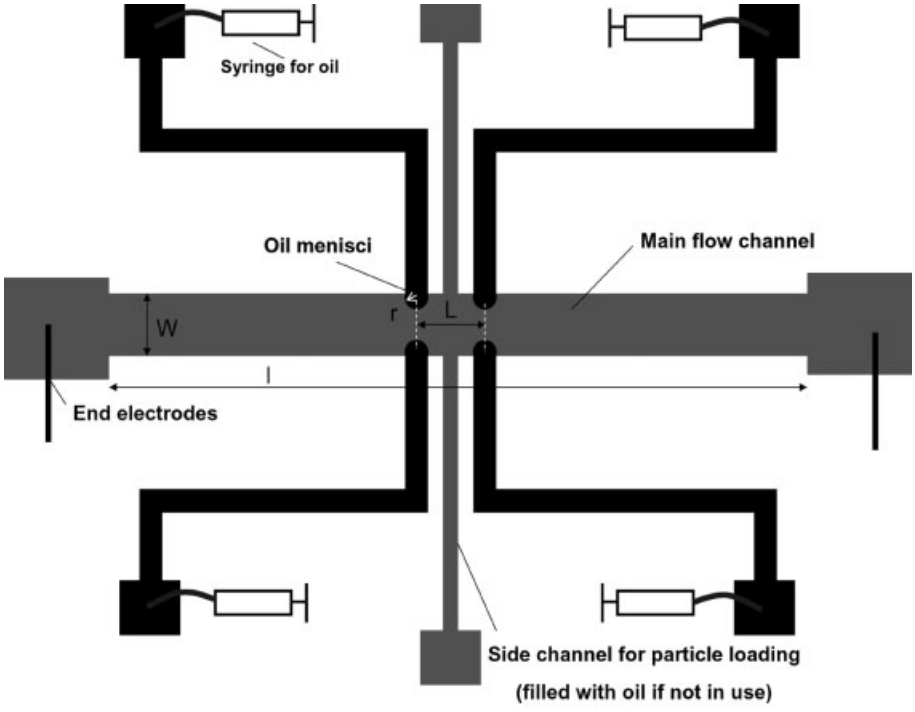

Figure 1. Schematic of the PDMS-glass device used in this paper for forming 2-D DEP potential well by applying DC electric field.

to a constant DC potential applied across the channel and produce a spatially nonuniform electric field in the region adjacent to them. Figure 2a shows the spatial profile of the energy due to the nonuniform field illustrating the large field gradients near the menisci. The sharply curved electric field lines and the spatially confined field gradients give rise to a DEP force on particles that have different conductivity than the suspending medium. The simulated DEP force field experienced by nonconductive particles due to such high field gradients is shown in Fig. 2b. The n-DEP forces push the particles away from both the menisci and towards the center of the channel. These lateral forces due to DEP, oriented in the plane perpendicular to that of the flow, act on the particles simultaneously along with the longitudinal pressure forces.

When the longitudinal forces are small, the large n-DEP forces from both sides push the particles towards the center of the channel where the velocity of the fluid is maximal and so they are accelerated along the direction perpendicular to the original flow axis. Such repulsive forces due to n-DEP acting on the particles originating from both the sides, force the initially dispersed particles to move in a single file, almost along the central flow streamlines, and thus mimic a focusing effect. We observed that this focusing is symmetrical about the axis perpendicular to flow, as the particles moving across the channel due to pressure-driven flow approaching the opposing oil menisci from both the directions exhibited similar focusing as they exited the menisci region (Fig. 3). It can also be noted that the focused stream of particles is about 70 μm wide about the flow axis. In flows

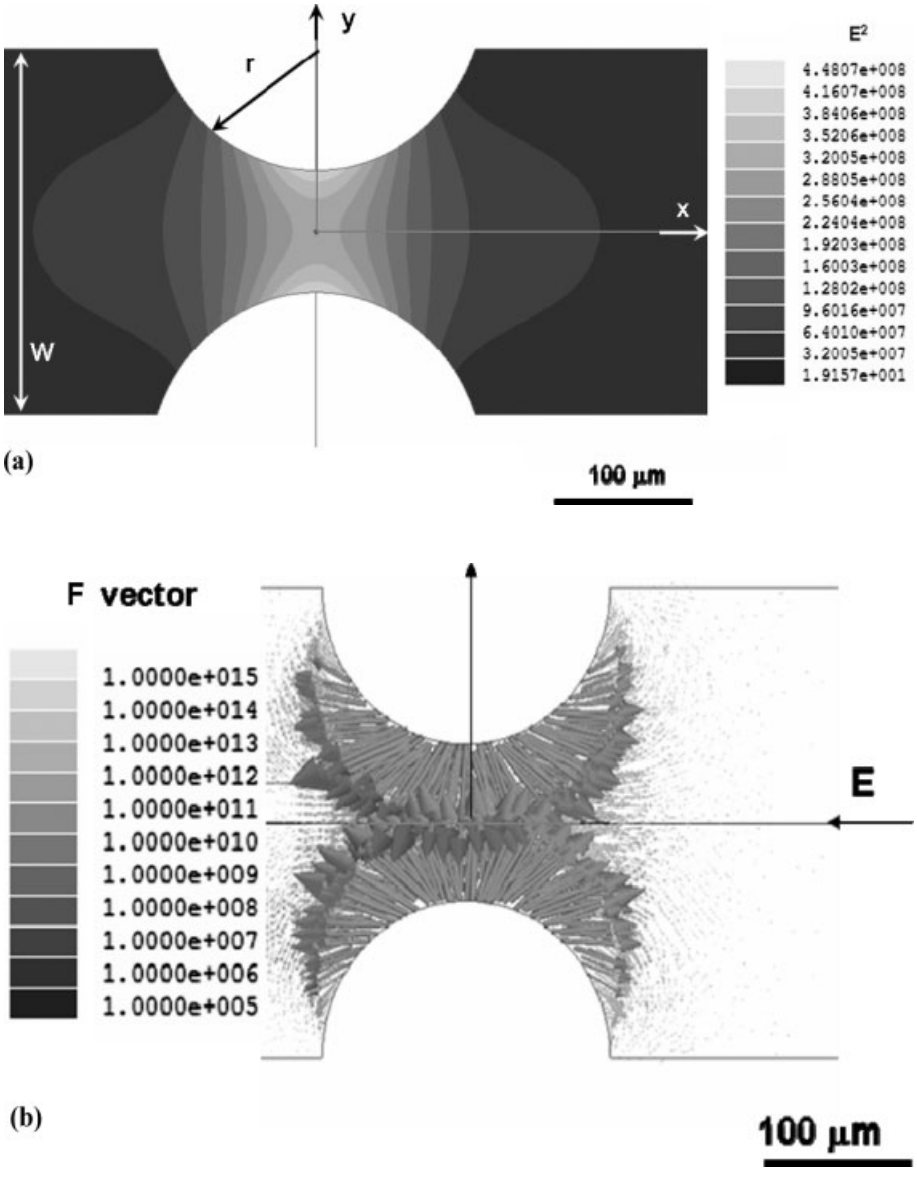

Figure 2. (a) Simulation results showing the spatial profile of energy ($\mathbf{E}^2$) due to the field shaping of the insulating oil menisci in creating a 1-D DEP potential field. (b) Simulation data illustrating the focusing forces due to n-DEP originating from the menisci and acting towards the center of the channel. The units of **F** vector are in units of field gradients as V^2/m^3.

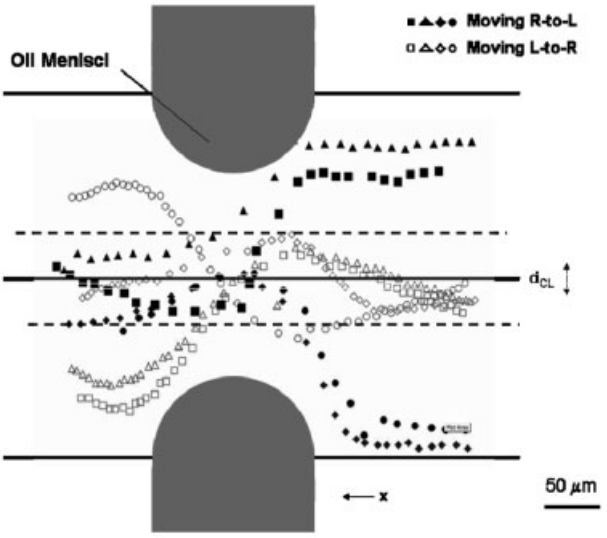

Figure 3. Trajectories of 10 μm green fluorescent carboxylate-modified polystyrene particles, observed at 0.1 s time interval, electrophoresing under DC field of 200 V/cm demonstrating the focusing effect of the 1-D DEP potential well. The dotted lines are visual guides to show the focused region of width around 75 μm. d_{CL} is the distance from the central axis. The trajectory data are drawn to scale on both axes.

with low *Re*, the focused stream of particles continues to remain focused due to the minimal mixing between different velocity streams of the fluid. In our experiments, $Re \sim 0.15$ which is in the laminar regime. This method of focusing can be used to enrich particulate streams or cell suspensions as an alternative to hydrodynamic focusing using sheath flows. Since the oil menisci can be retracted to any degree, the degree of focusing also can also be controlled.

While one pair of menisci produces a focusing effect, placing two such pairs adjacent to each other results in a trapping effect. Two pairs of insulating oil menisci, facing each other and oriented at 180° or 90° to each other create a spatially nonuniform electric field (Fig. 4a) and in turn produce large DEP forces. When nonconductive particles enter the gap between the two pairs of menisci, they experience n-DEP forces directed outwards from the insulating oil menisci and towards the center of the gap between the menisci pairs (Fig. 4b). Such a potential well confined spatially in the dimensions perpendicular to flow can be used for many trapping and concentrating applications. Figure 5 compares the simulated energy fields ($\mathbf{E}^2$ on *y*-axis) produced by quadrupolar electrodes and two pairs of oil menisci in quadrupolar geometry. The voltages used in the simulation for quadrupolar electrodes (+500 and −500 V) and DC field strength (50 V/cm for the case of two pairs of oil menisci) are chosen arbitrarily, but reflect typical experimental values. The similar profile of the energy wells indicates that the forces (proportional to $\nabla\mathbf{E}^2$) are comparable in shape and magnitude.

4.2 Engineering the DEP trap

In designing a DEP trap, one must balance the forces described in Eq. (4). In Fig. 6, a DC field of 300 V/cm was applied across the 5 cm flow channel to produce field gradients ($\nabla\mathbf{E}^2 \sim 3 \times 10^{13}$ V^2/m^3) high enough to create a DEP well that a 10 μm polystyrene particle carried by the crossflow is strongly held against the flow. For the conditions used in the experiment ($\sigma_p = 0.2 \times 10^{-3}$ S/m; $\sigma_m = 0.05$ S/m; CM = −0.5), the n-DEP forces were calculated to be ∼15–20 pN and the drag forces estimated from the flow conditions were also ∼18–20 pN ($v_{max} = 200$ μm/s). If the trap is weak, these forces will detach the particle from the region. We found that when the electric field is turned off, the particle is immediately detached from the trap and carried by the crossflow (data not shown). We also observed that the DEP repulsive barrier at the entrance to the well and between a pair of menisci can be very large so as to prevent any particle entering the trap region. Hence, for single particle trapping, it is preferable to keep the crossflow minimal and to turn on the trap by turning the DC field only when the particle is already in the region between the two pairs of menisci. Once the particle is inside the DEP trap, it may undergo small range movement if the relative magnitudes of the forces due to destabilizing crossflows and Brownian motion are comparable to the trapping forces.

Since the geometry of the DEP well is highly dependent upon the field gradients produced, field shaping by the oil menisci can be regulated to produce desired results. The extent of penetration of the oil menisci into the main flow channel determines the gap between the menisci and also the shape and magnitude of the field gradients produced around the region. Hence, by adjusting the penetration of oil menisci through pressure applied at the oil inlet ports, we can dynamically control the nature of the DEP trap formed between the pairs of menisci. We demonstrate this through an experiment where the concentration of 1 μm fluorescent particles trapped in the central circular region of radius 200 μm in the DEP trap is measured by monitoring the fluorescent emission against a dark background while one of the menisci is adjusted (Fig. 7). When the extent of penetration of the meniscus into the channel is increased, the field lines are compressed through an increasingly thinner gap between the menisci and so the DEP well becomes increasingly deeper resulting in increasingly more trapped particles. When the meniscus is withdrawn back, the DEP well became shallower resulting in the release of particles in the trap. This was shown in the plot as the decrease in fluorescence when *h* was decreased.

4.3 Simulation results: Parameters for future design

We performed simulations to understand the influence of different geometrical parameters on the dimensions of the DEP potential well and to guide the design of trapping potential wells of different dimensions for different trapping

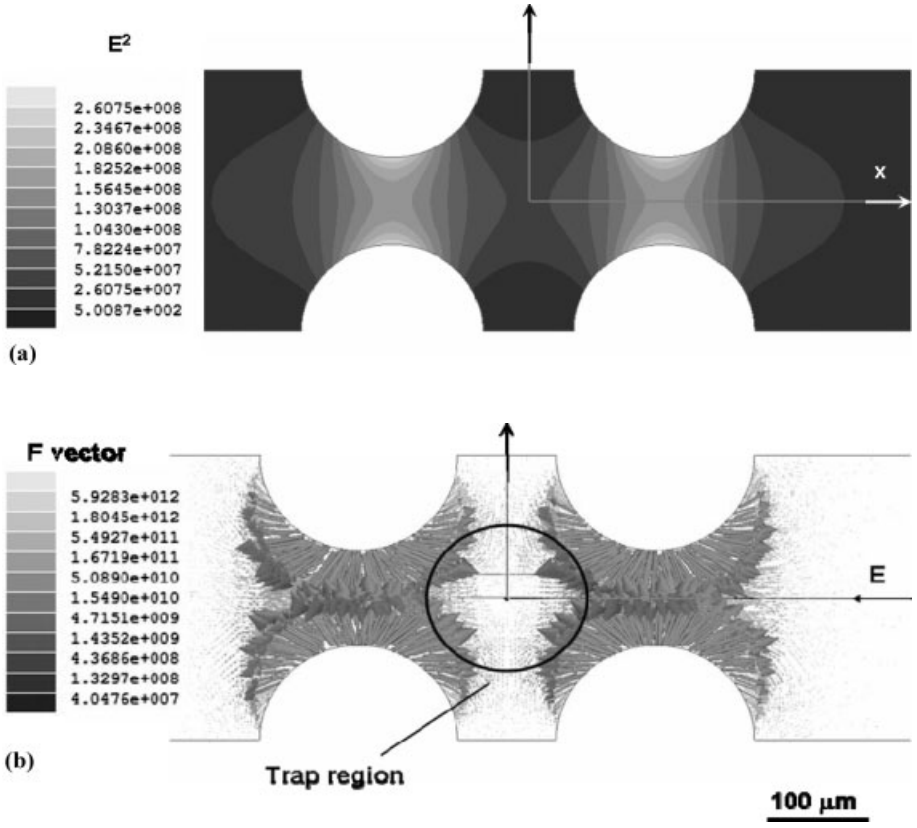

Figure 4. (a) Simulation results showing the spatial profile of energy ($\mathbf{E}^2$) due to the field shaping by two pairs of oil menisci in creating a 2-D DEP potential field. (b) Simulation data illustrating the forces due to n-DEP directed outwards from the menisci and hence creating 2-D DEP potential well at the center of the gap between the two menisci pairs.

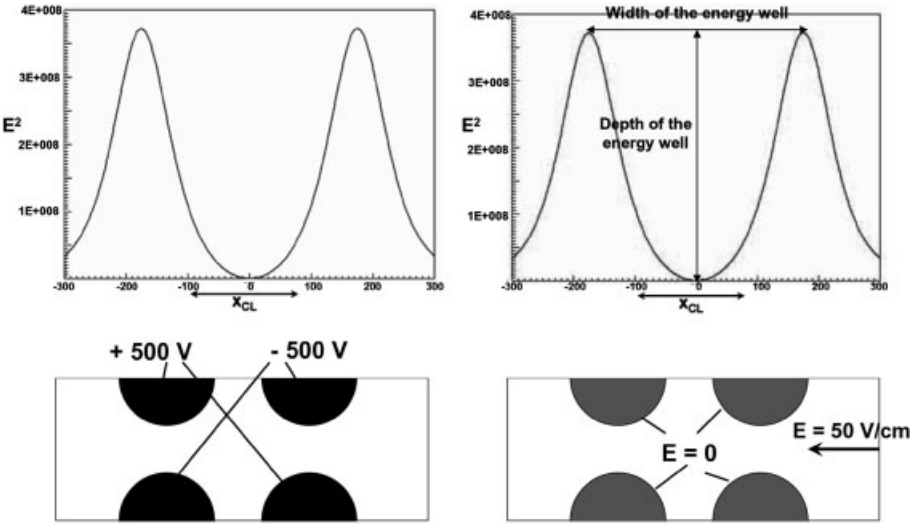

Figure 5. Comparison of the energy profiles produced by four electrodes in quadrupolar geometry and two pairs of oil menisci. The electrodes (shown in black) are shaped to match with the oil menisci (shown in gray). The shapes of the potential wells are comparable. x_{CL} is the distance along the central axis. The units of $\mathbf{E}^2$ in *y*-axis is V^2/m^2.

applications. For example, trapping a single particle requires the potential well to be deeper and narrower. We define a dimensionless parameter Θ to capture this property of the trap as

$$\Theta = \frac{\left(\text{Width of energy well}/\lambda\right)}{\left(\text{Depth of energy well}/\mathrm{E}_{\mathrm{DC}}^2\right)} \quad (10)$$

where the width of the energy well is the distance between the two energy barriers seen in the two-pair DEP energy well with the units of length, the depth of the energy well is the energy difference between the top and bottom of the DEP well with the units of V^2/m^2 (both illustrated in Fig. 5), $\mathbf{E}_{DC}$ is the applied uniform DC field in V/m and λ is the relevant characteristic length of the channel. We studied the effect of the radius of menisci (*r*) and the gap between the menisci

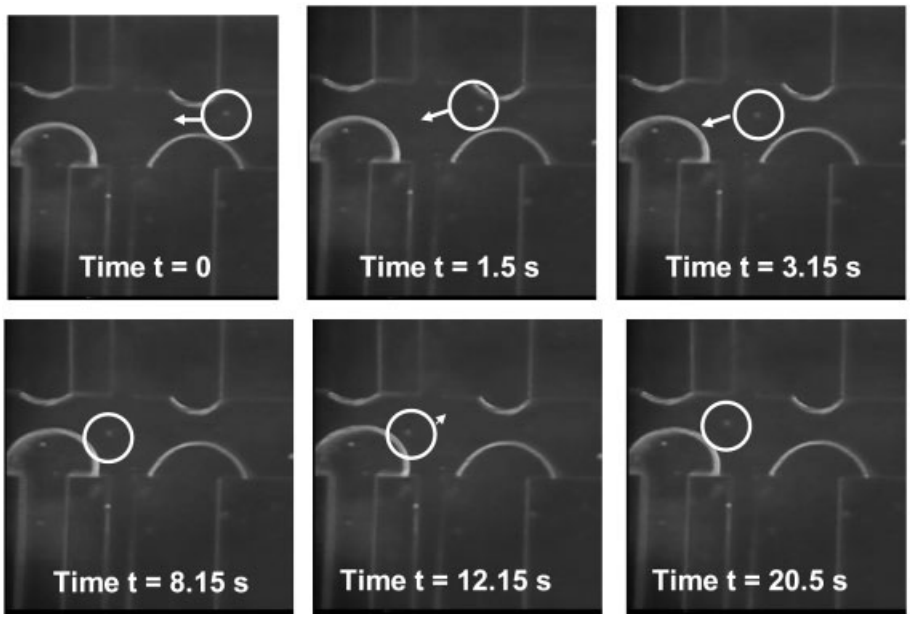

Figure 6. Time-sequence pictures of a single 10 μm green fluorescent carboxylate-modified polystyrene particle trapped in the 2-D DEP trap when applied DC field is 300 V/cm. The particle is shown encircled in the figures.

pair (L) on Θ. The relevant characteristic lengths are the width of the channel (W) and the total length of the channel along which the DC potential was applied (l) respectively for the two cases. To differentiate Θ calculated with the appropriate characteristic lengths for both the cases, we use Θ_L and Θ_r. Smaller values of Θ are preferred for single particle trapping. It is to be noted that Θ is only a descriptor of the potential well. The actual trapping forces scale as the cubic power of particle size (Eq. 2).

Figures 8a and b show the effect of the normalized gap between the pairs of menisci, L/W, and normalized radius of the oil menisci, r/W, on Θ, respectively. The linear fits ($r^2 = 0.99$) in both the cases show that changing the trapping geometry (characterized by L and r) proportionately alters the dimensions of the well (characterized by Θ. As L increases, the well becomes shallower and the DEP holding force (gradient of energy) becomes weaker proportionately. Hence, for holding particles against strong destabilizing flows, the menisci pairs need to be placed close to each other. Similarly, when the radius of the menisci is too small, the perturbation caused by the field-shaping insulating oil barrier is weak and hence the DEP potential well is shallow and wide resulting in small holding forces. The scaling relations (determined by fitting a linear equation to the simulation data) that can be useful in designing DEP traps of specific sensitivity, defined by Θ, are given as

$$\frac{L}{W} = 18.02\Theta_L - 0.62 \tag{11}$$

$$\left(\frac{r}{W}\right) = 0.49 - 0.59\Theta_r \tag{12}$$

Since the penetration of the oil menisci can be adjusted to vary the radius of curvature of the menisci over a range between 0 and r, a particular design geometry will still offer the possibility of creating DEP traps with a wide range of Θ_r.

An order of magnitude for Θ can be estimated using Eq. (3) by considering the perfect trapping of a single particle in a conservative force field (no frictional dissipation) where the width of the DEP well matches the diameter of the particle. For the case of trapping a single particle of 20 μm diameter against a crossflow that is 100 times stronger than the Brownian force at $T = 298$ K on a microfluidic channel of 2 mm length and 300 μm width and when a DC field of 1000 V/m is applied, Θ_L is 0.0541 and Θ_r is 0.36.

5 Concluding remarks

In this paper, we have developed a novel trapping method that does not require microfabricated electrodes to create the spatial nonuniformity of electric field. Insulating oil barriers are used instead to produce similar effects. This electrodeless approach eliminates expensive and time-consuming metallization and wet-etching processes typically required for patterning microelectrodes and hence facilitates rapid prototyping and testing of ideas. The elimination of the need for high-frequency AC circuits is another big advantage of our system especially for cases where the difference in conductivities between the sample and the medium is large. The insulating barriers made of oil offer the flexibility of dynamic control of the dimensions of DEP trap in the middle of an experiment through simple adjustment of the menisci (radii and extent of penetration). Unlike conventional electrode-based trapping methods, where reusability of the chips is limited by fouling and corrosion of electrode surfaces due to surface adsorption and electrolysis, the insulating oil can be changed multiple times. Such dynamic controllability, reconfigurability, and reusability are unique to this trapping method.

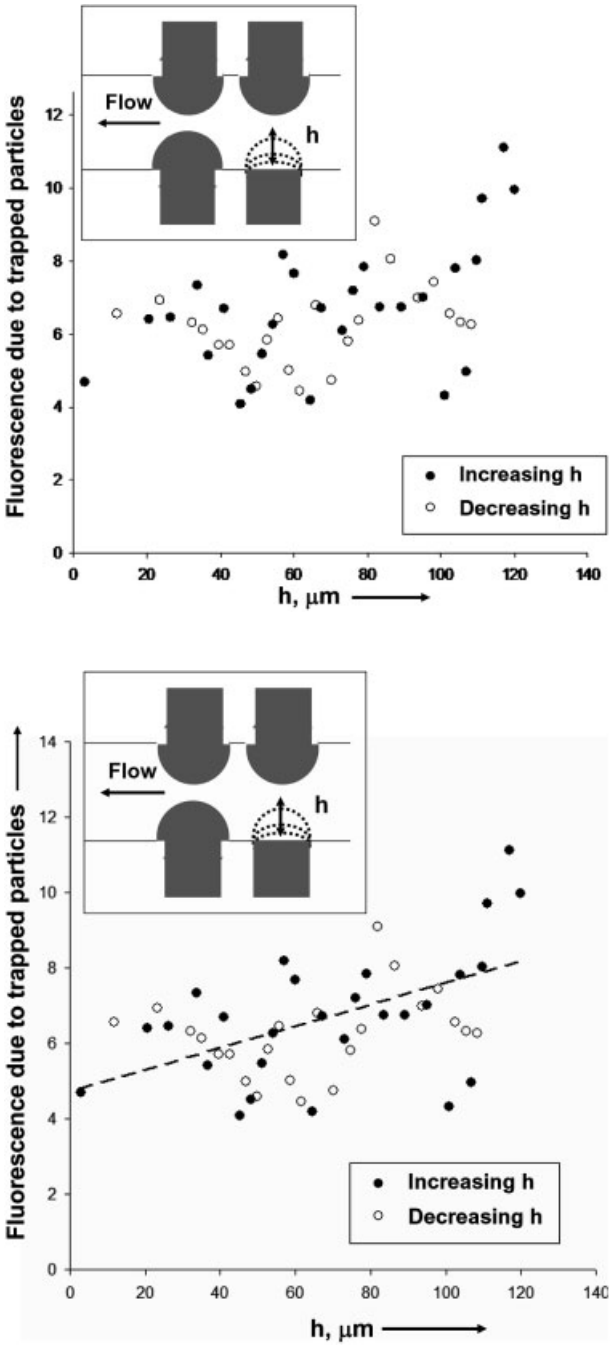

Figure 7. Change in concentration of 1.0 μm YG fluorescent polystyrene particles in a circular region of diameter ~200 μm in the center of the gap between the four insulating oil menisci in response to increasing and decreasing the extent of penetration (*h*) of one of the menisci into the main flow channel. The particles were too small to map the fluorescent intensity observed to the exact number of particles. The dotted line shows the trend line with the slope of 0.03.

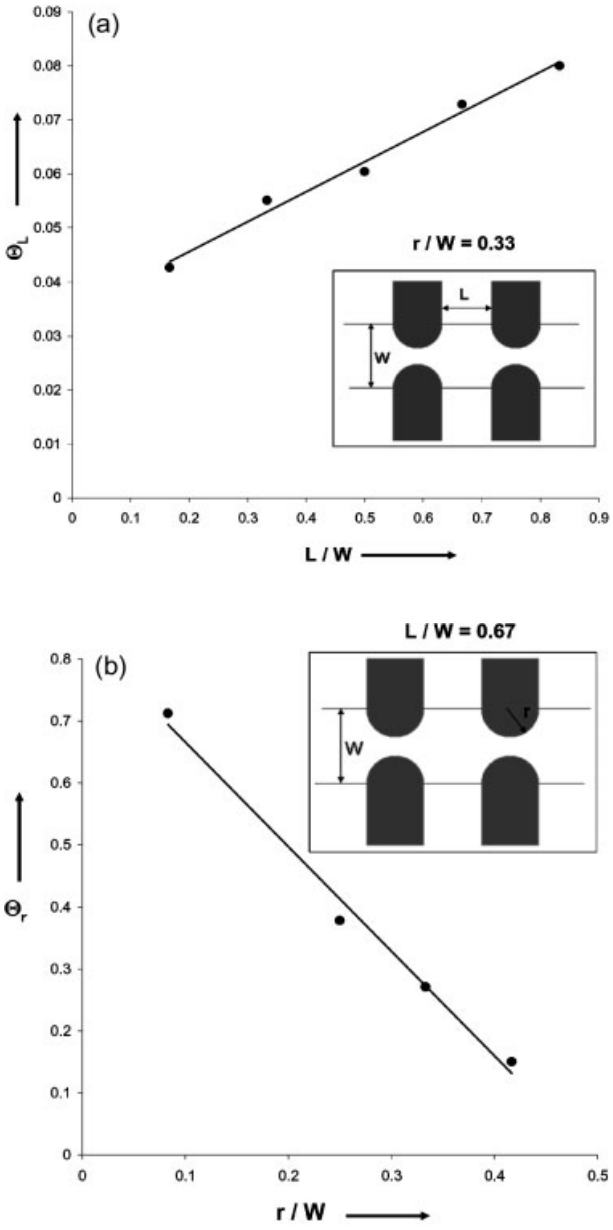

Figure 8. (a) Simulation results showing the variation of the Θ_L with the gap (*L*) between the adjacent oil menisci. The DC field used for the simulations was 100 V/cm. The radius of the oil menisci (*r*) is 100 μm and the width of the channel (*W*) is 300 μm for these simulations. The straight line is a linear fit (R^2 = 0.99) to the data. (b) Simulation results showing the variation of the Θ_r with the radius of curvature (*r*) of the oil menisci. The gap between the adjacent oil menisci is 200 μm and the width of the main channel is 300 μm for these simulations. The straight line is a linear fit (R^2 = 0.99) to the data.

We identified a design parameter Θ for characterizing the dimensions of the DEP trap and through simulations we developed correlations that can be used to design the geometry of the trapping conditions to produce traps of particular sensitivity. Simple particle trapping experiments as illustrated in the paper can be used to verify these simulations results. Though we demonstrated only n-DEP traps in this paper, our concept could also be used to fractionate different

particles in a suspension using p-DEP. In applications involving conductive particles like DNA, proteins, and some types of cells the particles would be more conductive than the suspending medium and would experience strong attractive DEP forces towards the interface resulting in their accumulation at the oil interface.

6 References

[1] Fiedler, S., Shirley, S. G., Schnelle, T., Fuhr, G., *Anal. Chem.* 1998, *70*, 1909–1915.

[2] Asbury, C. L., Diercks, A. H., van den Engh, G., *Electrophoresis* 2002, *23*, 2658–2666.

[3] Gascoyne, P. R., Vykoukal, J. V., Schwartz, J. A., Anderson, T. J. *et al.*, *Lab Chip* 2004, *4*, 299–309.

[4] Lapizco-Encinas, B. H., Simmons, B. A., Cummings, E. B., Fintschenko, Y., *Anal. Chem.* 2004, *76*, 1571–1579.

[5] Lagally, E. T., Lee, S. H., Soh, H. T., *Lab Chip* 2005, *5*, 1053–1058.

[6] Lumsdon, S. O., Scott, D. M., *Langmuir* 2005, *21*, 4874–4880.

[7] Zhiqiang, Z., Xiaolin, Z., Jiangong, X., Jianguo, C. *et al.*, *Conf. Proc. IEEE Eng. Med. Biol. Soc.* 2005, *2*, 1282–1285.

[8] Gadish, N., Voldman, J., *Anal. Chem.* 2006, *78*, 7870–7876.

[9] Hunt, T. P., Westervelt, R. M., *Biomed. Microdevices* 2006, *8*, 227–230.

[10] Lin, R. Z., Ho, C. T., Liu, C. H., Chang, H. Y., *Biotechnol. J.* 2006, *1*, 949–957.

[11] Schwartz, J. A., Vykoukal, J. V., Gascoyne, P. R., *Lab Chip* 2004, *4*, 11–17.

[12] Pohl, H. A., Crane, J. S., *Biophys. J.* 1971, *11*, 711–727.

[13] Fuhr, G., Arnold, W. M., Hagedorn, R., Muller, T. *et al.*, *Biochim. Biophys. Acta* 1992, *1108*, 215–223.

[14] Mahaworasilpa, T. L., Coster, H. G., George, E. P., *Biochim. Biophys. Acta* 1994, *1193*, 118–126.

[15] Washizu, M., Jones, T. B., *J. Electrostat.* 1994, *33*, 187–198.

[16] Goater, A. D., Pethig, R., *Parasitology* 1998, *117*, S177–S189.

[17] Schnelle, T., Müller, T., Fiedler, S., Fuhr, G., *J. Electrostat.* 1999, *46*, 13–28.

[18] Gimsa, J., *Bioelectrochemistry* 2001, *54*, 23–31.

[19] Chou, C. F., Tegenfeldt, J. O., Bakajin, O., Chan, S. S. *et al.*, *Biophys. J.* 2002, *83*, 2170–2179.

[20] Jones, T. B., *IEEE Eng. Med. Biol. Mag.* 2003, *22*, 33–42.

[21] Muller, T., Pfennig, A., Klein, P., Gradl, G. *et al.*, *IEEE Eng. Med. Biol. Mag.* 2003, *22*, 51–61.

[22] Voldman, J., Toner, M., Gray, M. L., Schmidt, M. A., *J. Electrostat.* 2003, *57*, 69–90.

[23] Bhatt, K. H., Velev, O. D., *Langmuir* 2004, *20*, 467–476.

[24] Hakoda, M., Hachisu, T., Wakizaka, Y., Mii, S., Kitajima, N., *Biotechnol. Prog.* 2005, *21*, 1748–1753.

[25] Hu, X., Bessette, P. H., Qian, J., Meinhart, C. D. *et al.*, *Proc. Natl. Acad. Sci. USA* 2005, *102*, 15757–15761.

[26] Singh, P., Aubry, N., *Phys. Rev. E Stat. Nonlin Soft Matter Phys.* 2005, *72*, 016602.

[27] Ahmed, R., Jones, T. B., *J. Electrostat.* 2006, *64*, 543–549.

[28] Forry, S. P., Reyes, D. R., Gaitan, M., Locascio, L. E., *J. Am. Chem. Soc.* 2006, *128*, 13678–13679.

[29] Ho, C. T., Lin, R. Z., Chang, W. Y., Chang, H. Y., Liu, C. H., *Lab Chip* 2006, *6*, 724–734.

[30] Kang, K. H., Kang, Y., Xuan, X., Li, D., *Electrophoresis* 2006, *27*, 694–702.

[31] Singh, P., Aubry, N., *Electrophoresis* 2007, *28*, 644–657.

[32] Jones, T. B., Washizu, M., *J. Electrostat.* 1996, *37*, 121–134.

[33] Morgan, H., Hughes, M. P., Green, N. G., *Biophys. J.* 1999, *77*, 516–525.

[34] Voldman, J., Braff, R. A., Toner, M., Gray, M. L., Schmidt, M. A., *Biophys. J.* 2001, *80*, 531–541.

[35] Suehiro, J., Hamada, R., Noutomi, D., Shutou, M., Hara, M., *J. Electrostat.* 2003, *57*, 157–168.

[36] Yang, L., Banada, P. P., Chatni, M. R., Lim, K. S. *et al.*, *Lab Chip* 2006, *6*, 896–905.

[37] Debesset, S., Hayden, C. J., Dalton, C., Eijkel, J. C. T., Manz, A., *Lab Chip* 2004, *6*, 396–400.

[38] Mpholo, M., Smith, C. G., Brown, A. B. D., *Sens. Actuators B* 2003, *92*, 262–268.

[39] Markx, G. H., Rousselet, J., Pethig, R., *J. Liq. Chromatogr. Relat. Technol.* 1997, *20*, 2857–2872.

[40] Masuda, S., Washizu, T., Nanba, T., *IEEE Trans. Ind. Appl.* 1989, *25*, 732–737.

[41] Cummings, E. B., Singh, A. K., *Anal. Chem.* 2003, *75*, 4724–4731.

[42] Ying, L., White, S., Bruckbauer, A., Meadows, L. *et al.*, *Biophys. J.* 2004, *86*, 1018–1027.

[43] Clarke, R. W., White, S., Zhou, D., Ying, L., Klenerman, D., *Angew. Chem.* 2005, *44*, 3747–3750.

[44] Zhou, G., Imamura, M., Suehiro, J., Hara, M., *IEEE Ann. Meeting Ind. Appl. Soc.* 2002, *2*, 1404–1411.

[45] Suehiro, J., Zhou, G., Imamura, M., Hara, M., *IEEE Ann. Meeting Ind. Appl. Soc.* 2003, *39*, 1514–1521.

[46] Lapizco-Encinas, B. H., Simmons, B. A., Cummings, E. B., Fintschenko, Y., *Electrophoresis* 2004, *25*, 1695–1704.

[47] Lapizco-Encinas, B. H., Davalos, R. V., Simmons, B. A., Cummings, E. B., Fintschenko, Y., *J. Microbiol. Methods* 2005, *62*, 317–326.

[48] Zhang, L., Tatar, F., Turmezi, P., Bastemeijer, J. *et al.*, *J. Phys. Conf. Ser.* 2006, *34*, 527–532.

[49] Barbulovic-Nad, I., Xuan, X., Lee, J. S., Li, D., *Lab Chip* 2006, *6*, 274–279.

[50] Demierre, N., Braschler, T., Linderholm, P., Seger, U. *et al.*, *Lab Chip* 2007, *7*, 355–365.

